JOURNAL OF CATALYSIS 83, 336–345 (1983)

Measurement of the Morphology of High Surface Area Solids: Porosimetry of Agglomerated Particles

WM. C. CONNER,[1] A. M. LANE, K. M. NG, AND M. GOLDBLATT

Department of Chemical Engineering, The University of Massachusetts, Amherst, Massachusetts 01002

Received February 16, 1983; revised May 3, 1983

Mercury intrusion porosimetry is a primary method of characterizing the morphology of high surface area solids. Based on a series of pressed microspheres, we have developed a three-dimensional interconnected network model for the void structure. As contrasted to the conventional model involving nonintersecting cylindrical pores (which are neither), a new perspective on porosimetry is discussed. Intrusion is controlled by constrictions, "throats," in the structure and extrusion is controlled by openings, "pores," in the structure. Because porosimetry is sequential, there is statistical deviation between the actual and measured "throats" and "pores." This comparison between scanning porosimetry data and the simulation of porosimetry provides a consistent method for interpreting the morphology of agglomerated particles.

INTRODUCTION

Mercury porosimetry as developed by Ritter and Drake (*1, 2*) in 1945 has become a commonplace technique for determining the pore-size distribution of porous solids and catalysts in particular. As suggested by Washburn (*3*) the pore structure is usually assumed to be made of cylindrical, nonintersecting capillary tubes. Mercury will penetrate a pore at a pressure corresponding to the pore radius according to the Washburn equation

$$Pr = -2\gamma \cos \theta$$

where P is the pressure, r is the radius, γ is the surface tension, and θ is the wetting angle. As pressure is increased, pores of proportionally smaller radius are filled and a volume distribution of pore sizes can be determined.

This interpretation of pressure/volume data is a well-recognized oversimplification. Many attempts have been made to develop a more reasonable analysis. Most, however, have dealt with large particle packings ($>10^4$ Å) applicable to soil engineering. We will deal exclusively with small particle agglomerates (<400 Å) of interest to those working with high surface area catalysts. In particular, any attempt to refine the analysis to obtain a more accurate pore size distribution must also account for extrusion hysteresis and mercury retention.

Some researchers have utilized a network of interconnected void spaces to represent the porous structure (*4*). Although hysteresis in contact angle has been suggested to explain porosimetry phenomena (*5, 6*) network effects and void geometry alone are sufficient to explain hysteresis and retention. A realistic model which is amenable to analysis is a packing of spheres.

A simple cubic packing is shown in Fig. 1. The pore space consists of the cavity centered between eight spheres. It is connected to other pores by the six throats or openings situated in the plane of four adjacent spheres.

Kruyer (*7*) studied the subatmospheric intrusion into 0.5–1.0 mm particles and concluded that intrusion is determined by the size of the throats and extrusion by the size of the pores. Other investigations (*8,–10*) have refined this analysis by more care-

[1] To whom correspondence should be addressed.

0021-9517/83 $3.00
Copyright © 1983 by Academic Press, Inc.
All rights of reproduction in any form reserved.

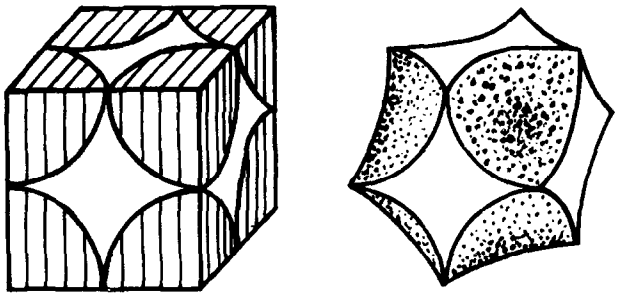

FIG. 1. Simple cubic packing of spheres: a unit cell is depicted on the left and the void space on the right.

fully relating the throat geometry to breakthrough pressure and including the filling of the toroidal volume around the contact points of spheres. These studies were conducted on 40–70 mesh spheres.

Network effects, which are statistical in nature, were first noticed by Meyer (*11*) who proposed a probablistic method for correcting pore size distributions for rock-like samples. Recently Doe and Haynes (*12*) attempted to apply empirical corrections to size distributions. The influence of other factors such as pore to throat ratio, coordination number, nonrandom heterogeneities and sample size have also been investigated (*13*). Networks are particularly amenable to analysis by percolation techniques as shown by Wall and Brown (*14*).

In spite of the amount of analysis done on mercury porosimetry, very little has been incorporated into routine practice (*15*). It will be the ultimate purpose of our research to gain a better understanding of porosimetry. We hope to develop methods by which a more complete and accurate description of the pore morphology can be obtained without substantial extra effort on the part of the analyst.

Recently scanning porosimetry has become available (from Quantachrome, Inc.). In this technique, a hydraulic ram exerts a continuously increasing pressure of mercury on the sample, yielding a continuous pressure/volume curve. We have utilized this technique to study the pore structure of a series of compacted microspheres from 70 to 400 Å in diameter. The experimental approach was to develop a series of well-characterized pore structures by compacting these microspheres to a void fraction around 50%. These can be reasonably approximated as a cubic lattice. The porosimetry results were simulated using a three-dimensional network of pores interconnected by throats. Relationships between actual and measured throat and pore size distributions could then be drawn.

EXPERIMENTAL

Microspheres (Degussa Aerosils) between 70 Å (7 nm) and 400 Å (40 nm) nominal diameter (as reported by Degussa) were compressed at increasing pressure from 1000 to 30,000 psig in a cylindrical 1-in.^{2} die. After compaction, the sample was broken into pieces approximately 1–2 mm in size and evacuated at less than 200 μm. Intrusion and extrusion porosimetry of these samples was performed on a Quantachrome Autoscan porosimeter using triple-distilled mercury.

The individual microspheres are not porous. Conventional BET surface area measurements were also conducted on both pressed and unpressed samples. As expected the surface area decreased by about 10% as the area of contact between spheres increased.

The porosimeter measurements were simulated by computer. The simulation was based on a three-dimensional network of in-

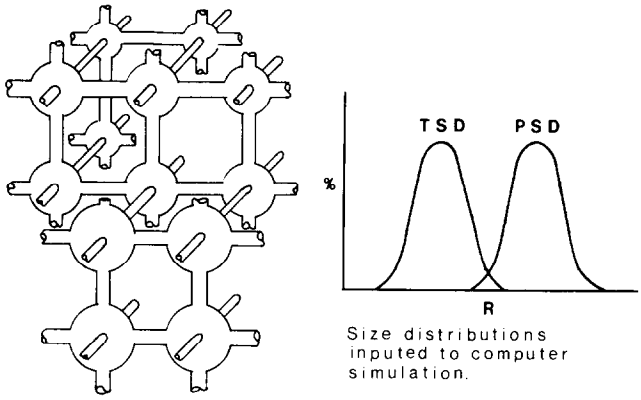

FIG. 2. Three-dimensional pore/throat network: throat and pore sizes are assigned at random from a Gaussian distribution.

terconnected pores and throats as represented in Fig. 2. This is a model of the void space only; the solid structure that gives rise to the void space is not shown. The spheres represent the void openings (pores) and the connecting tubes represent the void constrictions (throats). The pores and throat dimensions were generated from a Gaussian size distribution and assigned at random throughout the network at the intersections and interconnections, respectively. These dimensions represent the critical (or controlling) radius of the pores and throats. The model and simulation are discussed in more detail in our first paper (*16*). Based on the simulation the relationship between the actual and measured pore and throat size was analyzed.

RESULTS

Figure 3 shows the effect of compaction pressure on the porosimetry (intrusion and extrusion) of samples of the 70-Å particle. As expected the pressures required for intrusion and extrusion increased with the pressure of compression (i.e., the "radius" decreased). Some drift after the extrusion experiment reached 0 pressure was observed. This is why the reintrusion curve does not start at the same point as the extrusion curve ends. We have not fully explained this.

In Table 1 we show the effect of compression on the most probable radius of intrusion and extrusion for the smallest 70-Å particle. In addition the void fraction is shown—calculated from the known density of the silica (2.2 g/cm^3) and the measured volume intruded for each sample. As seen a void fraction of around 0.5 was found for compression around 20–30,000 psig.

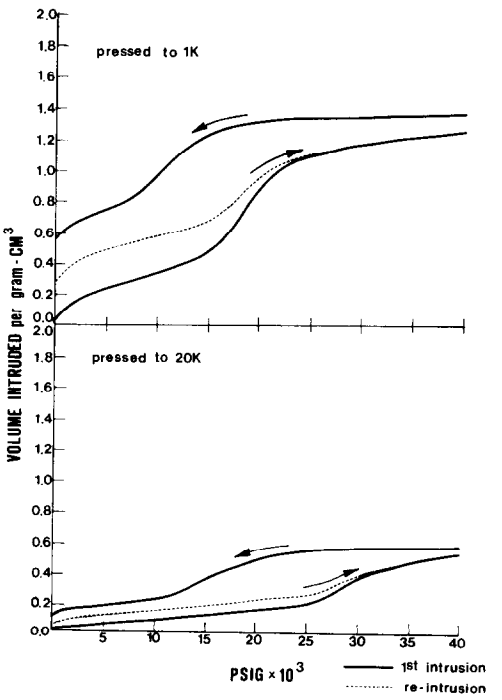

FIG. 3. Porosimetry of Aerosil 380 pressed to 1K and 20K psi.

TABLE 1

Aerosil 380

Pressed to a pressure of (psia)	Most probable $\langle r_i \rangle$ Intrusion	Most probable $\langle r_e \rangle$ Extrusion	Void fraction	$\langle r_e \rangle / \langle r_i \rangle$
1,000	57 Å	122	0.73	2.2
10,000	42.5	100	0.64	2.3
20,000	37	84	0.57	2.3
30,000	32	72	0.51	2.3

A series of aerosils with varying particle size was studied. The intrusion and extrusion derivative curves for three of these agglomerates (identified by nominal particle diameter) are seen in Fig. 4.

Table 2 summarizes the data collected on the series of compressed microspheres. The series span spheres between 7 and 32 nm in nominal particle diameter and 360 and 43 m^2/g surface area. The most probable radius for intrusion and extrusion (corresponding to the maximum of the derivative (dv/dr) curves) are listed. A wetting angle of 130° was used to calculate the relationship between pressure and radius. The ratio of the measured most probable radii of extrusion, RE, and intrusion, RI, is listed: the ratio is obviously independent of wetting angles. The ratio (≈2.2–2.3) seems characteristic of packed spheres. Equivalent ratio's for other silicas varied between 7.5 and 1.5. This possible method of classifying void structure will be discussed in a later publication.

The surface area as measured by BET–nitrogen adsorption is shown. The surface area is also calculated by the simple relationship applicable for cylindrical pores (i.e., $A = 2V/r_i$). This calculation often differs significantly from and is larger than the measured surface area. Since the volume intruded and the BET surface area are measured parameters, the discrepancy probably lies with the radius used in the calculation. Specifically, the radius of intrusion is too small a value, yielding an erroneously high surface area. This will be discussed in the next section.

From the BET surface area, the average particle sizes can be calculated, and are shown. Based on a cubic array of particles the minimum diagonal distance (throat diameter) between particles in a plane is calculated ($2r(\sqrt{2} - 1)$). The size of the unit

TABLE 2

Morphological Characterization (Porosimetry and Surface Area) of Compacted Microspheres[a]

	Measured				Calculated			
	Intrusion radius	Extrusion radius	r_e/r_i	Surface area BET	Surface area ($2v/r_i$)	Particle radius	Throat radius ($0.414r$)	Pore radius (r)
Ox 50	163	358	2.20	43	50	319	132	319
Mox 80	117	260	2.21	66	83	207	86	207
Aerosil 130	95	210	2.21	93	131	147	62	147
Aerosil 200	46	106	2.29	124	165	109	46	109
Aerosil R974	50	112	2.23	110	213	136	56	136
Aerosil R972	69	146	2.12	170	242	91	38	91
Aerosil R805	44	107	2.44	150	266	104	43	104
Aerosil H55	37	82	2.23	220	295	65	27	65
Aerosil R812	27	64	2.38	230	428	59	24	59
Aerosil 300	45	96	2.13	300	298	50	21	50
Aerosil 380	26	60	2.29	360	347	42	18	42

[a] Surface area in m^2/g and sizes in Å (see text).

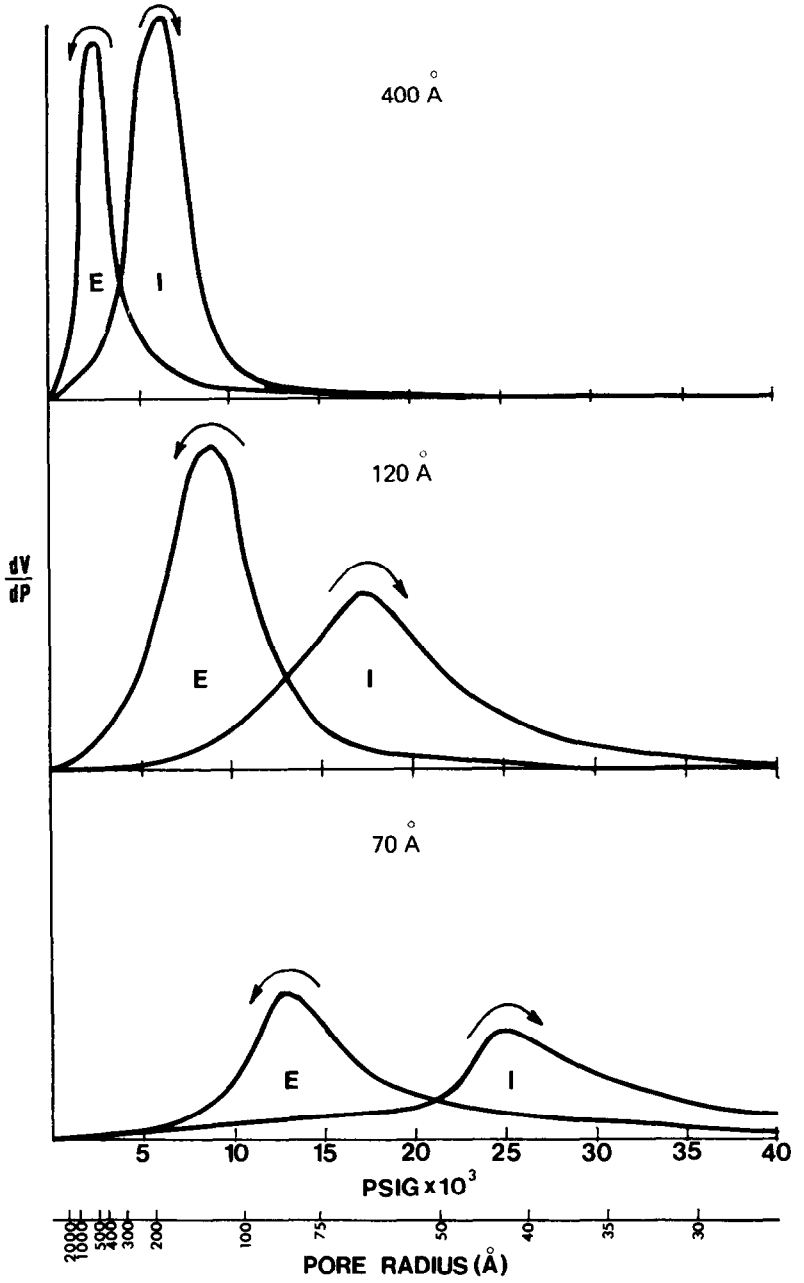

FIG. 4. Porosimetry of compressed (20K psi) microspheres: the derivatives of the intrusion and extrusion curves for different size microspheres.

cell ($2r$) is used to calculate a pore diameter. As is evident these compare reasonably with the measured throat and pore sizes—in view of the myriad of estimates and assumption.

The simulation of porosimetric measurement of the OX-50 is shown in Fig. 5 with the actual porosimeter scan of the sample. As is seen, the simulation reflects all the aspects of the measured spectra. The intru-

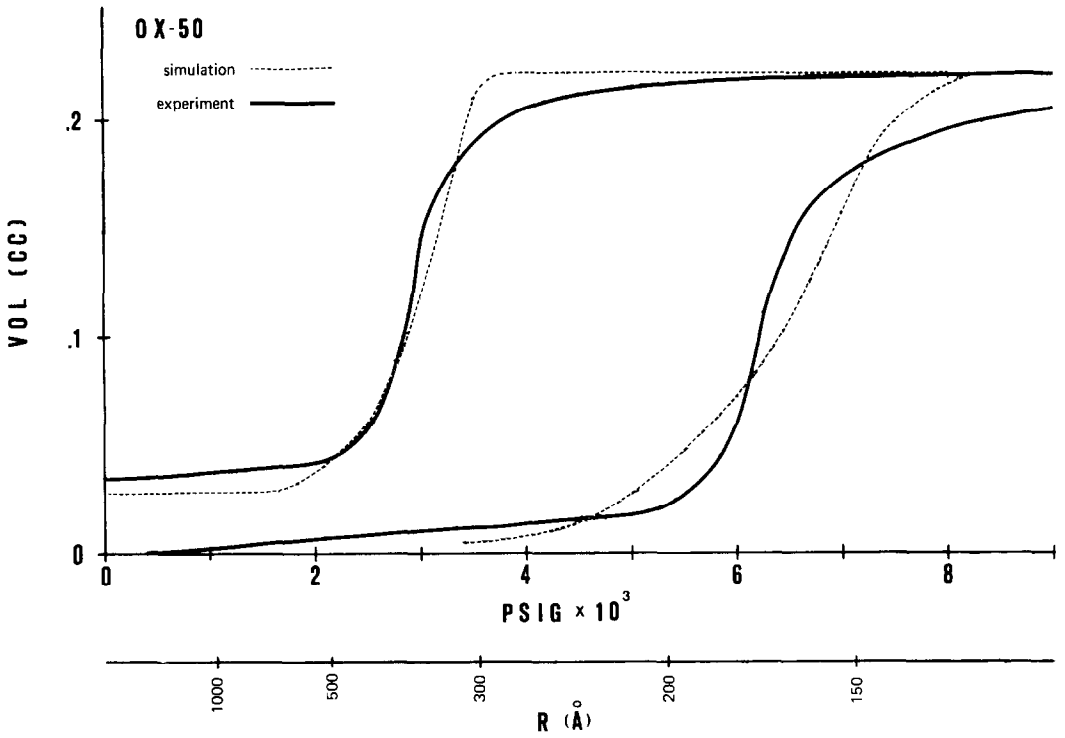

FIG. 5. Porosimetry of OX-50: experimental curves and overlay of the simulation.

sion and extrusion measurement as well as the volume of mercury retained are depicted in the simulation.

The actual pore and throat size distributions inputed to the computer simulation are not measured in the same way due to statistical reasons. Figures 6 and 7 show the throat and pore size distributions used in and measured by the simulation of OX-50. Of the throats assigned to the simulation (*actual*) only the largest are *penetrated* in such a way as to be measurable. When these throats are *measured* they appear to be slightly smaller than they actually are.

The pore size distribution imputed to the computer simulation (*actual*) is *measured* as narrower. Also, some of the larger pores are not measured at all because they become *stranded* in the porous matrix. The reasons for these shifts will be discussed in the next section.

DISCUSSION

To understand the measurement of solid structure and the actual morphology, it is necessary to measure a series of known solid structures. By utilizing a series of agglomerated (pressed) microspheres this was done. The void fraction will depend on the pressure of agglomeration. This was seen (Fig. 3 and Table 1). At a void fraction of 0.5 the solid structure can be approximated by cubic packing (*18*). The cubic packing in three dimensions results in an interconnected void structure. The simplified reproducible unit cell for this structure was shown in Fig. 1 and discussed in the introduction.

A three-dimensional representation of interconnected pores and throats with an interconnectivity of six was easily simulated (*16*). This representation is able to recreate the intrusion and extrusion porosimetry measurements (Fig. 5). Explanation of the hysterisis between intrusion and extrusion based on structural vs "wetting angle shifts" (an alternative explanation) will be discussed in our subsequent publication

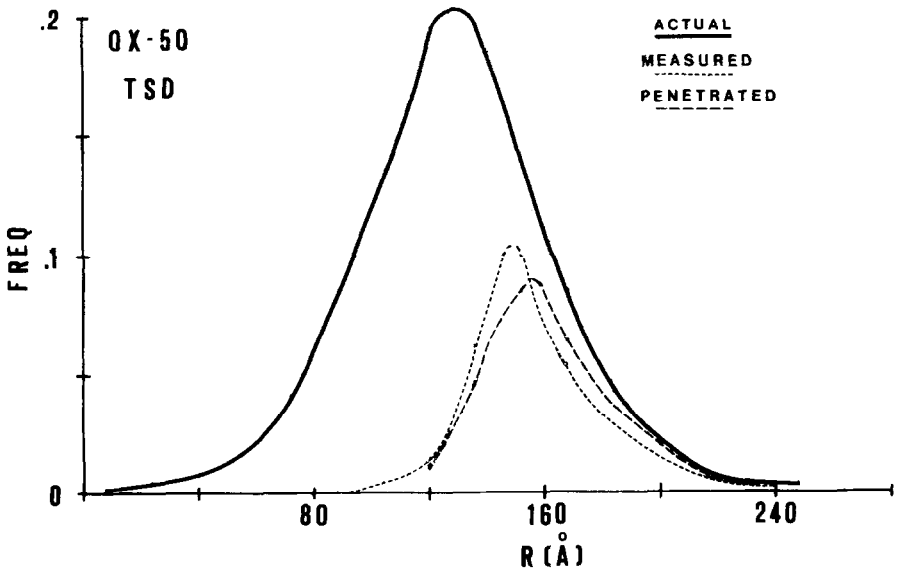

FIG. 6. Porosimetry of OX-50: simulation of the throat size distributions.

(*19*). For the purpose of the analysis we will assume that structural explanations dominate.

A critical conclusion is that the intrusion of mercury into the agglomerate structure is dictated by the throat size whereas the extrusion is controlled by the size of the pores. Both the experiments and the simulation confirm that indeed intrusion will depend on the constrictions of the solid struc-

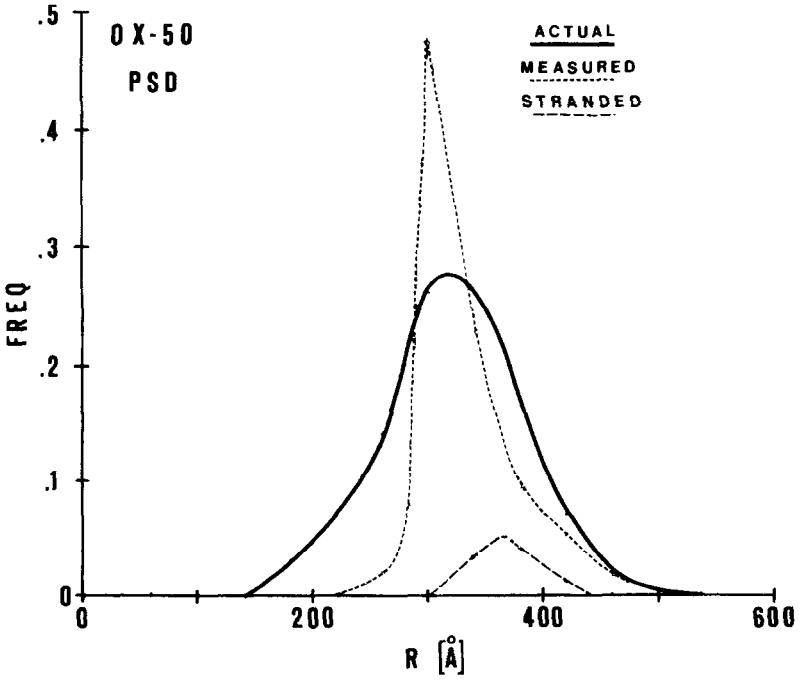

FIG. 7. Porosimetry of OX-50: simulation of the pore size distributions.

ture and extrusion will depend on the openings behind these constrictions. This is true for any agglomerate structure and not restricted to the present case. For any irregular agglomerate a pore and throat space can always be defined. When only the intrusion curve is used to characterize the solid structure, the picture is incomplete and incorrect.

As was seen in Figs. 6 and 7 the measured and actual distributions of throats and pores are different. It must be mentioned that we have not actually observed this in experiment but only in the computer simulation. In order to explain this phenomenon it is necessary to understand the sequential nature of porosimetry. Mercury invades the solid from the outside in and leaves from the inside out. Three phenomena contribute to deviation in the measurement: "shadowing," "nonlinkage," and "mercury retention."

Porosimetry during intrusion involves the sequential invasion of the pore structure by penetration through the throats. Not all throats of a proper size to be penetrated (hence, measured) are accessible at any time. Some of the throats are "shadowed" because they are not accessible until a pore to which the throat is connected has been filled. Throats, even large throats, at the interior of a particle are not measured until the adjoining pores have been invaded. After invasion of a throat into a specific pore, new throats are made accessible. If any of these throats are larger than the throat that was invaded they are also invaded, but they are measured at a pressure corresponding to the smaller throat of access. This shadowing will result in measuring throats as smaller than they actually are.

Because of the connectivity (number of throats to which each pore is connected to neighboring pores), it is not necessary to invade each throat to access each of the pores. Since the majority of the internal void space is found in the pores, only throats that access unfilled pores contribute significantly to the intruded volume vs pressure measurement. For a given connectivity, C, only $2/C$ of the throats are needed to access the pore (void) structure. For example, for our cubic packing with a connectivity of six, only one is needed to access each pore. Two-thirds of the throats are not measured (since each internal throat is shared by two pores, the numerical ratio of throats to pores is about 3). The throats that are not measured are "not linked" to empty pores or are too small to be measured. Since penetration will occur via the largest accessible throat, only the relatively large throats are measured.

These two phenomena, shadowing and nonlinkage, are depicted in Fig. 8. Three distributions are shown. The curve labeled "actual" represents the distribution of

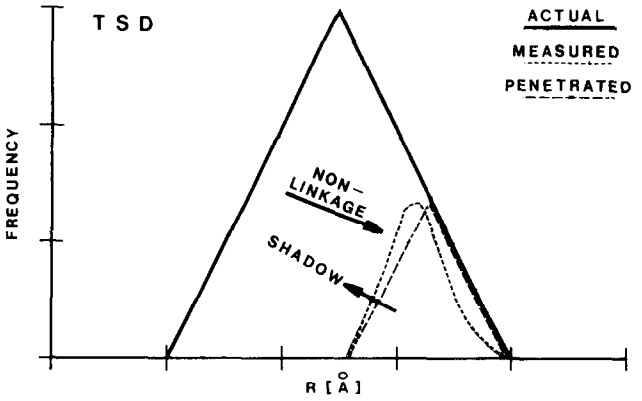

FIG. 8. Theoretical throat size distributions.

throats inputed to the computer simulation. The effect of nonlinkage is shown by the "penetrated" curve which is significantly shifted to reflect larger throats as invaded. Even though these throats are invaded, shadowing will shift the measurement again. The curve labeled "measured" reflects the combination of both nonlinkage and shadowing. It will be the distribution of throats measured during intrusion. The major effect is nonlinkage which dictates a larger and narrower throat size distribution than actual.

Extrusion involves the sequential evacuation of mercury from pore spaces. The retraction occurs away from a mercury/vacuum interface, such as a previously emptied neighboring pore or a broken thread of mercury in a narrow throat. Surface tension will in most cases dictate that the pores will not evacuate independently. In order for the mercury to leave a pore it must be connected to the outside by an unbroken mercury continuum.

During extrusion the pore size dictates the pressure necessary to vacate the void structure. Shadowing will also influence the measurement. A pore can only be emptied if an interface is available. After a pore evacuates, the pores to which it is connected have interfaces. If they are smaller but were not previously connected to an empty pore, they will empty. However, the pores will be measured at a pressure at which the larger interconnected pore became evacuated. More specifically small pores will be interpreted as larger than they actually are. This results in a shift between measured and actual pore size. The measurement of the "actual" distribution in Fig. 9 is shifted by the simulation to larger sizes.

During extrusion individual or interconnected groups of pores can become isolated. Either snap-off, where a small radius of curvature results in scission of the connection (throats) between pores can occur; or an individual or group of pores can be isolated from the receding mercury interface. For statistical reasons, a predominance of larger pores will be isolated. The "stranded" curve in Fig. 9 represents the stranded pore size distribution and shifts the measurement toward smaller sizes.

The combination of effects results in a narrowing of the measured distribution of pores: the smaller pores are not measured by shadowing and the larger pores are not measured by their propensity for isolation as retained mercury.

CONCLUSIONS OF THE ANALYSIS OF POROSIMETRY

Several conclusions can be drawn from the analysis as articulated above:

(1) For an agglomerate of interconnected

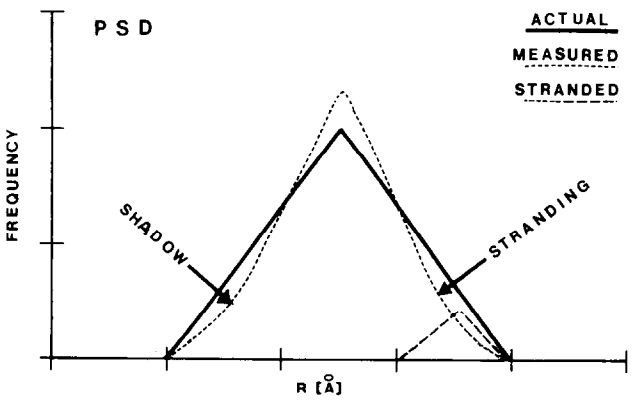

FIG. 9. Theoretical pore size distributions.

"pores" and "throats" intrusion is controlled by the throats and extrusion is controlled by the pores. A more complete analysis of the void structure is found by measuring both intrusion and extrusion.

(2) The statistics of porosimetry dictate that the throats will be smaller in size than those measured. The combination of shadowing and nonlinkage will result in a broader actual distribution of throats than measured.

(3) The distribution of pores as measured is narrower than the actual distribution. Both shadowing and mercury retention contribute to this deviation.

(4) Because the conventional interpretation depends on intrusion and this does not account for the pore size, the surface area will be calculated as larger than the actual surface area.

We have demonstrated that more and better information can be obtained from mercury porosimetry using a more realistic representation of the void structure than currently used. The derivative of the intrusion curve, usually taken to be the pore size distribution, will represent an "average" void size. This is because the measured throat size distribution lies between the actual pore and actual throat size distributions. This is merely a fortunate coincidence. To understand the morphology of complex interconnected void structures, it is necessary to analyze and understand the phenomena by which it is measured. This paper attempts to contribute to this understanding.

ACKNOWLEDGMENTS

We wish to thank the National Science Foundation for their donation of the equipment. We also thank Gulf Research and Development Corp. for their financial support of this research. Dr. J. Horowitz is thanked for his helpful discussion of statistics related to these studies.

REFERENCES

1. Ritter, H. L., and Drake, L. C., *Ind. Eng. Chem. Anal. Ed.* **17,** 782 (1945).
2. Drake, L. C., and Ritter, H. L., *Ind. Eng. Chem. Anal. Ed.* **17,** 787 (1945).
3. Washburn, E. W., *Proc. Natl. Acad. Sci. U.S.A.* **7,** 115 (1921).
4. Van Brakel, J., *Powder Technol.* **11,** 205 (1975).
5. Lowell, S., and Shields, J. E., *J. Colloid Interface Sci.* **83,** 273 (1981).
6. Kloubek, J., *Powder Technol.* **29,** 63 (1981).
7. Kruyer, S., *Trans. Faraday Soc.* **54,** 1758 (1958).
8. Freuel, L. K., and Kressley, L. J., *Anal. Chem.* **35,** 1492 (1963).
9. Mayer, R. P., and Stowe, R. A., *J. Colloid Sci.* **20,** 893 (1965).
10. Mayer, R. P., and Stowe, R. A., *J. Phys. Chem.* **70,** 3867 (1966).
11. Meyer, H. I., *J. Appl. Phys.* **24,** 510 (1953).
12. Doe, P. H., and Haynes, J. M., *Charact. Porous Solids, Proc. Symp.* 253 (1978).
13. Wardlaw, N. C., and McKellar, M., *Powder Technol.* **29,** 127 (1981).
14. Wall, G. C., and Brown, R. J. C., *J. Colloid Interface Sci.* **82,** 141 (1981).
15. Moscou, L., and Lab, S., *Powder Technol.* **29,** 45 (1981).
16. Lane, A. M., Ng, K. M., Conner, W. C., and Lapidus, G. R., *Chem. Eng. Sci.*, submitted, 1983.
17. Gregg, S. J., and Sing, K. W. W., "Adsorption, Surface Area and Porosity," p. 182. Academic Press, New York, 1967.
18. Graton, L. C., and Fraser, H. H., *J. Geol.* **43,** 785 (1935).
19. Conner, W. C., Lane, A. M., and Hoffman, A. J., *J. Colloid Interface Sci.*, submitted, 1983.